Climate mode impacts on the sea surface height anomaly in the Indian Ocean

Xiaolin Zhang[1] and Takashi Mochizuki[1]

1. Department of Earth and Planetary Sciences, Kyushu University, 744 Motooka, Nishi-ku, Fukuoka 819-0395, Japan

Index: Indian Ocean SSHA, Climate Modes, Rossby Waves, Surface Heat Flux

To be submitted to Geophysical Research Letters

Corresponding author: Xiaolin Zhang, Takashi Mochizuki

Email: xz12j@my.fsu.edu, mochizuki.takashi.817@m.kyushu-u.ac.jp

Abstract

We examine observational data to clarify impacts of three major climate modes on Sea Surface Height Anomaly (SSHA) of the Indian Ocean during 1993-2016: The El Niño and Southern Oscillation (ENSO), the Indian Ocean Dipole mode (IOD) and the Asian summer monsoon. ENSO and IOD dominantly control the SSHA in the eastern tropical area and in the western tropical and northwestern areas of the Indian Ocean, respectively, while the monsoon contributes to local SSHA.

For all climate modes, SSHA is primarily linked to the wind-forced ocean upwelling. In particular, the trade-wind and alongshore-wind changes associated with ENSO- and IOD-related atmospheric convection clearly control the equatorial and coastal upwelling of the tropical areas. The net heat flux anomaly at the sea surface always works to damp the tropical SSHAs. In the northwestern areas, on the other hand, it can contribute to enhancing the SSHAs relevant to IOD and monsoon.

1. Introduction

Sea Surface Height Anomaly (SSHA) can be measured by satellite in recent years. This allows us to better understand the ocean circulation, predict short and long term effects of the weather and the earth's climate over time. It is also important to the navigation, fisheries management and offshore operations. SSHA can be forced by wind stress, heat flux and freshwater. The wind stress leads to Ekman convergence, inducing thermocline upwelling (characterized by changes of 20°C isothermal layer depth, D20 hereafter) and SSHA. Hence upwelling (D20 shoaling) and SSHA are closely linked to each other; thus, they have been studied in connection or separately. Surface heat flux produces baroclinic pressure signals in the upper ocean with horizontal scale larger than the baroclinic radius of deformation; such pressure signals can be mostly retained locally, giving rise to regional SSHA signals (Huang and Jin, 2002). The freshwater flux gives rise to barotropic pressure signals, which are quickly dispersed into the world oceans, leaving negligible signals in SSHA (Huang and Jin, 2002).

Another effect of freshwater flux is the mixing of the freshwater into the isothermal layer of the ocean, which will lead to a shallower mixed layer depth, that will further lead to the existence of barrier layer (see Zhang and Clarke, 2015).

> The Indian Ocean is subject to seasonal monsoon forcing (Schott and McCreary,

2001 and Schott et al. 2009). During the summer season, northeasterly wind prevails in the Northern Indian Ocean and during the winter season southeasterly wind blows. In contrast, the southern Indian Ocean is subject to yearly steady southeasterly wind forcing. In response to the wind stress forcing, seasonal upwelling appears along eastern Indian coast and the western Indian Ocean, the thermocline dome exists south of the equator through the whole year. Wind stress forcing in the Indian Ocean has strong interannual variability in forms of two climate modes, El Niño and Southern Ocean (ENSO) and Indian Ocean Dipole Mode (IOD), and they play different roles in the eastern Indian Ocean and western Indian Ocean. Yu et al. (2005) shows that north of 10°S, IOD dominates; however, ENSO is more important for the latitude band of 14°S-6°S. A few mechanism has been discussed in terms of the mechanisms of Indian Ocean thermocline upwelling (or the anomaly of D20). Tozuka et al. (2010) suggests that the interannual D20 anomaly (D20A) in the western Indian Ocean upwelling zone is primarily caused by Rossby waves generated by winds in the central and eastern Indian Ocean; in addition, local Ekman pumping also contribute. The influence of remote forcing from the Pacific via the Indonesian Throughflow is weak in this area, even though it has significant contributions in the southeast Indian Ocean (e.g., Potemra 2001; Trenary and Han 2012; Deepa et al. 2018; Hu et al. 2019). In fact, Rossby waves play an important role in regulating interannual variability of sea level over the south Indian Ocean (Woodberry et al. 1989; Périgaud and Delecluse 1992, 1993; Zhuang et al. 2013).

Although the impacts of ENSO and IOD have been studied extensively, the role of

monsoon has not been fully addressed. For example, how much the monsoon contributes to the eastern and western Indian Ocean SSHA. Moreover, how the surface heat flux will impact SSHA remains unclear. Figure5 from Zhang and Han (2020) suggests that if the monsoon is cut off from the forcing, the model cannot explain the observed sea level signals, especially in the northeastern Indian Ocean. In this study, we will firstly explore the spatial pattern of SSHA induced by wind stress, heat flux forcing and fresh water flux. Second, we will discuss the role of monsoon in the Indian Ocean SSHA.

The remain part of this paper is as follows. Section 2 describes the data sets and

methodology. Section 3 compares the Indian Ocean SSHA during El Niño, positive IOD and Section 4 investigates the impact of climate modes (ENSO, IOD and monsoon) on SSHA. Section 5 discusses the mechanism related to

each forcing (wind stress, heat flux and freshwater flux). Section 6 estimates the contribution of each climate modes on the *in-situ* sea level along Arabian Sea, Section7 summarizes the results.

1. Data Sets and Methodology

1. *Sea Surface Height*

The SSHA datasets are the 1/4° monthly Archiving, Validation, and Interpretation of Satellite Oceanography (AVISO) data from 1993 to 2016.

1. *D20*

The depth of 20°C isotherm (D20, representing the thermocline depth), that reflects the contribution of wind-forced SSHA (or upwelling), is calculated from the monthly temperature data of European Center for Medium-Range Weather Forecast (ECMWF) Ocean Reanalysis System 4 (ORAS4) available for 1958–2016 (Balmaseda et al. 2013).

1. *Net heatflux data*

To examine the heat flux caused SSHA, the net heat flux (available from January 1984 to December 2009) on a 1°x1° spatial grid is from the Objective Analysis Flux (OAFlux; Yu & Weller, 2007). The net heat flux data is a combination of OAFlux and the International Satellite Cloud Climatology Project (ISCCP), positive means downward. The net shortwave and longwave radiation results are from ISCCP.

1. *Wind stress data*

The monthly wind stress data (resolution of 0.75°) is available from European Center for Medium-Range Weather Forecast (ECMWF) dataset.

1. *In-situ Sea Level Data*

To estimate the climate modes' impact on sea level along the eastern coast of Arabian Sea, we also used the *in situ* sea level data from permanent service for mean sea level. Our discussion will be mainly focused on the following three stations: Masirah, Muscat and Salalah.

Major El Niño events and positive IOD events for the period of January 1993 to December 2016 are identified according to the indexes published in the National Oceanic and Atmospheric Administration (NOAA) website (https://origin.cpc.ncep.noaa.gov/products/analysis_monitoring/ensostuff/ONI_v5.php) and the Australian government Bureau of Meteorology website (http://www.bom.gov.au/climate/iod/). The Indian monsoon index is downloaded from the following website (http://climexp.knmi.nl/dat2nc.cgi?datafile=data/pALLIN.dat&type=p&station=All-India_Rainfall&id=someone@somewhere). The sea surface temperature (SST) used to estimate the climate mode index since 1870 to present is available from the Hadley Centre Global Sea Ice and Sea Surface Temperature (HadISST) dataset (Rayner et al. 2003).

Here the monthly anomaly is estimated by removing the mean seasonal cycle. For example, January anomaly is estimated by removing seasonal mean of January for all the years (1993-2016). A Trenberth filter has been used to calculate the interannual variability of the time series (Trenberth, 1984).

In order to estimate the contribution of each climate mode (ENSO, IOD and monsoon) on Indian Ocean SSHA, we used a 'static' linear regression model as following (see also Zhang and Han, 2020).

$Y(t) = b_0 + b_1 X_1(t) + \varepsilon_t$ (1)

Here Y(t) is the time series of SSHA averaged in each boxed region as defined in the following text, b_0, b_1 are constants, X_1 is the time series of different climate mode index; for instance, the Nov.-Jan. averaged ENSO index (Niño3.4), Sept.-Nov. (SON) averaged IOD index (DMI), and Jun.-Aug. (JJA) averaged monsoon index are used here, and ε_t represents an error term

In the following sections, we will try to estimate the impacts of different climate modes (ENSO, IOD and monsoon) on the Indian Ocean SSHA and the spatial pattern of wind stress, freshwater flux, surface heat flux related SSHA.

1. **Composite of Indian Ocean SSHA during El Niño, positive IOD**

TableS1 shows the major El Niño and positive IOD events since 1993 January as defined by NOAA website (from Zhang and Han, 2020). We can see that for the period of 1993 January to 2016 December there are 7 El Niño events, 5 positive IOD events; there are 4 El Niño events co-occur with positive IOD events. To explore the impact of different climate modes on Indian Ocean SSHA, we composite the SSHA in the Indian Ocean for all the pure El Niño years (2002, 2004, 2009), all the pure positive IOD years (2012) and the co-occur years (1994, 1997, 2006, 2015) for the period of 1993 January to 2016 December (see Figure1). It is clear that during co-occur years, the SSHA shows a typical positive IOD pattern, namely negative SSHA along the eastern Indian coast and positive SSHA in the western Indian Ocean. Alongshore southeasterly winds also appear in the eastern Indian Ocean. During positive El Niño years, positive SSHA appears in the western Indian Ocean, along the equator and eastern Indian coast. Negative SSHA is in the southern Indian Ocean and northern Indian ocean. Associated with the positive SSHA in the eastern Indian Ocean is the northwesterly wind prevailing along the eastern coast (Figure1a). Different from the pure El Niño years, during the pure positive IOD years, negative SSHA appears in the western Indian Ocean and along the equator (about -1.5cm). Figure1d is the composite of SSHA for the rest of the years (or defined as independent years), which shows a positive SSHA (about 1cm) in the eastern Indian Ocean and negative SSHA (around -1cm) in the western Indian Ocean. The amplitude of which is much smaller than the co-occur years, pure El Niño years and pure positive IOD years. Figure1 indicates that the El Niño and IOD events have different impact on the pattern of Indian Ocean SSHA. Here the composite of SSHA during El Niño years is estimated based

on Nov.-Jan. (NDJ) average and the composite of SSHA during IOD years is based on Sept.-Nov. (SON) average.

FigureS1 is the time series of yearly ENSO, IOD and Monsoon index for the period of 1993 January to 2016 December, which shows that ENSO index is slightly correlated with IOD index, with a correlation of 0.61 ($r_{crit}95\%$=0.49) (FigureS1a). ENSO index is also correlated with Monsoon index with a correlation of -0.17 ($r_{crit}95\%$=0.53) (FigureS1b). Here the yearly ENSO index is defined as the Nov.-Jan. mean Niño3.4, IOD index is defined as the Sept.-Nov. average DMI index and monsoon index is averaged from Jun.-Aug. From FigureS1, we conclude that although ENSO has an impact on Indian monsoon, they are slightly different. Furthermore, ENSO has a period of 3-7years, however, monsoon is a semiannual variability. The spatial pattern of Indian SSHA related to ENSO, IOD and monsoon expected to be different. In the following section, we will try to estimate the contribution of different climate modes (ENSO, IOD and monsoon) on the Indian ocean SSHA.

1. **The impact of climate modes on SSHA**

In order to explore the spatial pattern of SSHA corresponding to each climate mode forcing, we regressed ENSO, IOD and monsoon index on Indian Ocean SSHA (Figure2). As suggested by previous research, in the eastern Indian Ocean, mainly ENSO and IOD play a role, in the western Indian Ocean, both ENSO and IOD contributes (see also Zhang and Han, 2020). The correlation map of ENSO, IOD and monsoon with Indian Ocean SSHA further suggests that monsoon mainly has an impact in the northwestern and western Indian Ocean (see Figure2b-e). To further quantify contribution of ENSO, IOD and monsoon, we defined three box regions, namely, western Indian Ocean box (WIO, bounded by 50°E-80°E, 12°S to 2°S), eastern Indian Ocean box (EIO, bounded by 90°E-115°E, 10°S-0°N) and Northwestern Indian Ocean box region (NWIO, bounded by 60°E-78°E, 2°N-15°N). By using the 'static' linear regression model as described in Eq.(1), we conclude that in the WIO, ENSO is the most important, in the EIO, IOD is dominant and in the NWIO, ENSO is most important. The standard deviation of ENSO, IOD and monsoon contribution is 2.63cm, 2.43cm, 0.38cm for WIO, 1.69cm, 2.29cm, 0.35cm for EIO, 1.69cm, 0.96cm, 0.12cm for NWIO (see FigureS2).

So far, we have discussed the contributions of each climate modes on Indian Ocean SSHA, in the following section, we will try to explore the mechanisms that cause the SSHA pattern in the Indian ocean. More specifically we will discuss the climate modes (ENSO, IOD, and monsoon) related wind forcing, heat flux forcing and freshwater flux forcing contribution to the SSHA pattern in the Indian Ocean.

1. **Mechanisms**

As discussed in the previous text, SSHA is mainly caused by three mechanisms, wind stress forcing, heat flux forcing and fresh water flux forcing. The wind stress can cause local Ekman pumping and excite Rossby waves that will fur-

ther cause the change of D20A (see Eq. 15 in Qiu (2002)). This also refers to 'upwelling' in oceanography. The heat flux will change the SSHA by heating (cooling) the surface ocean. For instance, if there is a net heat flux from atmosphere to ocean, the ocean will expand, which will lead to a positive SSHA. The freshwater flux can change SSHA in two ways. Firstly, adding water into the ocean will generate barotropic gravity waves, that can propagate globally in a few weeks and the net SSHA is negligible (see Huang and Jin, 2002). Furthermore, the freshwater can be mixed into the ocean and change the stratification of the upper ocean. The SSHA related to this aspect is also very small in the western tropical Pacific Ocean (see Zhang and Clarke, 2016).

1. **Wind forced SSHA**

To evaluate the contribution of wind-forced SSHA (reflected by the change of D20) , we regressed the ENSO, IOD and monsoon index on the D20A in the Indian Ocean (see Figure3a-c). Similar to the spatial pattern of total SSHA (Figure2a-c), in the eastern Indian Ocean, ENSO and IOD dominate, in the western Indian Ocean, ENSO and IOD dominate, but ENSO is slightly more important (Figure3a-c). Correlation map suggests that monsoon mainly plays a role in the NWIO (FigureS3a-c). The difference between the spatial pattern of SSHA and D20A is caused by the heat flux forcing and fresh water flux. In the following, we will try to understand the process that contributes to the upwelling variability.

Since the D20A (or upwelling) in the open ocean is mainly caused by the Ekman pumping and propagation of Rossby waves (see Eq. 15 in Qiu, 2002). To explore the causes of Indian Ocean upwelling (or wind-forced SSHA) by different climate modes, we regressed outgoing longwave radiation (OLR), wind stress and Ekman Pumping on each climate indexes (ENSO, IOD, monsoon) (see Figure3d-f). Figure3d-f suggests that during El Niño and positive IOD events, the southeasterly wind stress along eastern coast (related to ENSO/IOD/monsoon) will drive Ekman transport (upwelling) that will cool the mixed layer ocean. This will further cause a negative SSHA. In the open ocean, during El Niño events, there will be drier anomaly in the eastern Indian Ocean and anomalous wetter in the west. This will drive an easterly wind anomaly along the equator (or weakend convection). The easterly wind stress is also associated with negative windstress curl anomaly in the eastern Indian Ocean, which will lead to local Ekman convergence, or upwelling in the eastern Indian Ocean. This signal will propagate westward and further shallower the thermocline in the west. In other words, in the western Indian ocean, the upwelling is caused by local Ekman pumping and westward propagation of Rossby waves. In the northwestern Indian Ocean region, similar to eastern Indian Coast, the along shore wind (seasonally changed due to the monsoon impact) will drive a semi-annual along shore upwelling. In the Arabian Sea, local Ekman convergence (divergence) and the coastal waves play the role of setting up the anomaly as in the other parts of the open ocean.

1. **Heat flux forced SSHA**

The surface heating can cause the expansion of upper ocean, leading to a positive SSHA. Such perturbations appear in the forms of baroclinic pressure anomaly in the upper ocean. Since the horizontal scale of heating is no larger than the baroclinic radius of deformation of the ocean, most signals will be retained locally after the adjustment (Huang and Jin, 2002). The cooling (heating) of the mixed layer ocean can further lead to an reduced (increased) $\frac{\rho}{\rho_1} = g'$, where $\rho = \rho_2$-ρ_1 is the difference of density between the mixed layer depth and lower layer, ρ_1 is the density of the lower layer ocean and g' is reduced gravity number. This suggests that $|dh/dx| \sim \sqrt{|W_e|/g'}$ (the slope of thermocline depth, We is Ekman pumping) will increase (decrease) and furthermore, for the north Indian Ocean, reduction in reduced gravity will lead to steeper thermocline, downwelling in the west and upwelling in the east. In the thermocline ridge (southern Indian Ocean), reduction in reduced gravity, will lead to steeper thermocline. Or in other words, deeper thermocline in the east and shallower thermocline in the west, which will be related to downwelling in the east and upwelling in the west.

The regression and correlation of surface net heat flux shows that during El Niño events a net heat release from ocean gives rise to negative SSHA in the NWIO. However, during positive IOD and monsoon season (June-August), the heat flux caused SSHA is positive due to the net heat into the ocean from the atmosphere (see Figure3g-i). In addition, in the eastern Indian Ocean, ENSO, IOD and monsoon are all related to a positive net heat flux into the ocean. This suggests that during El Niño, positive IOD and summer monsoon season (Jun.-Aug.), the heating of surface ocean will lead to a positive SSHA, and IOD will dominate (see Figure3g-i). In contrast, in the western Indian Ocean, the cooling of surface ocean leads to negative SSHA. Monsoon induced heat flux mainly contributes in the NWIO and EIO.

1. **Freshwater flux forced SSHA**

Freshwater flux in forms of precipitation adding to the ocean gives rise to barotropic pressure signals to the water column. Since the horizontal scale of precipitation is much smaller than the barotropic radius of deformation, most of the signals will be quickly dispersed into the world oceans, leaving negligible signals remain in the local oceanic region (Huang and Jin, 2002). The fresh water will further be mixed into the surface ocean, and will lead to a shallower (fresher) mixed layer and furthermore a barrier layer. The existing of barrier layer caused SSHA is also negligible even in the western tropical Pacific ocean (see Figure6, Zhang and Clarke, 2016). Quantification of this impact will be an interesting topic for our future research.

1. **ENSO/IOD/monsoon contribution to in situ sea level**

Long measurement of in situ sea level by tide gauge is available from permanent service data. Here we estimated the contribution of each climate modes (ENSO, IOD and monsoon) on the sea level at three stations (Muscat B, Masirah and Salalah) along the eastern coast of Arabian Sea for the period of 1993 January to 2016 December (see FigureS1 for the monthly anomaly). At station Masirah,

monsoon dominates, at station Muscat B, ENSO dominates, and at station Salalah, IOD dominates (see Figure4). Note here, the more complicate coastal dynamics is out of our scope.

1. **Summary and Discussion**

Using statistical linear regression model, we estimated the impacts of different climate modes (ENSO, IOD and monsoon) on the Indian Ocean SSHA. Our study suggests that in the Eastern Indian Ocean, IOD dominates, in the region of thermocline ridge of the Indian Ocean, ENSO dominates, in the Northwestern Indian Ocean, ENSO dominates. The standard deviation of monsoon contribution is 0.38cm for WIO, 0.35cm for EIO and 0.12cm for NWIO.

Along the eastern Indian coast, the SSHA is mainly driven by the wind. In the eastern Indian open ocean, the wind forcing caused Ekman convergence will drive upwelling (or negative SSHA) and it will propagate westward in the form of Rossby waves. In the western Indian ocean thermocline ridge region, the local Ekman pumping also contributes. In the northwestern Indian Ocean, the upwelling is mainly related to local Ekman pumping. The heat flux related SSHA is negative in the NWIO, which is linked to a net heat release from ocean during El Niño events. However, during positive IOD and summer monsoon season, the heat flux caused SSHA is positive due to the net heat into the ocean from the atmosphere. The freshwater flux caused SSHA is negligible since the barotropic waves will propagate globally in a weak. Lastly, by using in situ measurement of sea level data from permanent service data, our analysis further shows that at station Masirah, monsoon dominates, at station Muscat B, ENSO dominates, and at station Salalah, IOD dominates (see FigureS4). Note here we did not take into account of the diversity of ENSO events (in other words, separate El Niño events into central and eastern Pacific El Niño events) and the decadal shift of El Niño events as suggested by previous research (Bunge and Clarke, 2014). These will be interesting topics for future research.

Acknowledgments.

We gratefully acknowledge funding from the Japan Society for the Promotion of Science (JSPS) KAKENHI (grant JP19H05703). Discussions with Drs. Ruixin Huang, Mikhail karpytchev, Yu Kosaka help improve the paper significantly.

Data Availability Statement.

Data sets used in this study can be found at the following websites: AVISO SSHA: https://www.aviso.altimetry.fr/en/data.html. D20 is from ECMWF ORAS4 https://www.ecmwf.int/en/forecasts/dataset/ocean-reanalysis-system-4. ECMWF Windstress data: http://apps.ecmwf.int/datasets/. The net heat flux is from OAFlux: https://oaflux.whoi.edu/. In-situ Sea Level data is based on permanent service for mean sea level (https://www.psmsl.org/data/obtaining/map.html#plotTab).

References

Balmaseda, M. A., K. E. Trenberth, and E. Källén (2013), Distinctive climate signals in reanalysis of global ocean heat content, Geophys. Res. Lett., 40, 1754–1759, https://doi.org/10.1002/grl.50382.

Bunge, L., and A. J. Clarke (2014), On the warm water volume and its changing relationship with ENSO, J. Phys. Oceanogr., 44, 1372–1385, https://doi.org/10.1175/JPO-D-13-062.1.

Deepa, J. S., C. Gnanaseelan, R. Kakatkar, A. Parekh, and J. S. Chowdary (2018), The interannual sea level variability in the Indian Ocean as simulated by an ocean general circulation model, Int. J. Climatol., 38, 1132–1144, https://doi.org/10.1002/joc.5228.

Ebisuzaki, W. (1997), A method to estimate the statistical significance of a correlation when the data are serially correlated, J. Climate, 10, 2147–2153, https://doi.org/10.1175/1520-0442(1997)010%3C2147:AMTETS%3E2.0.CO;2.

Huang, R. X., and X. Jin (2002), Sea surface elevation and bottom pressure anomalies due to thermohaline forcing, Part I: Isolated perturbations, J. Phys. Oceanogr., 32, 2131–2150, doi:10.1175/1520-0485(2002)032<2131:SSEABP>2.0.CO;2.

Périgaud, C., and P. Delecluse (1992) Annual sea level variations in the southern tropical Indian Ocean from Geosat and shallow-water simulations, J. Geophys. Res., 97, 20169–20178, https://

doi.org/10.1029/92JC01961.

Périgaud, C., and P. Delecluse (1993) Interannual sea level variations in the tropical Indian Ocean from Geosat and shallow water simulations, J. Phys. Oceanogr., 23, 1916–1934, https://doi.org/10.1175/1520-0485(1993)023%3C1916:ISLVIT%3E2.0.CO;2.

Potemra, J. T. (2001) Contribution of equatorial Pacific winds to southern tropical Indian Ocean Rossby waves, J. Geophys. Res., 106, 2407–2422, https://doi.org/10.1029/1999JC000031.

Qiu, B. (2002) Large-scale variability in the midlatitude subtropical and subpolar North Pacific Ocean: Observations and causes, J. Phys. Oceanogr., 32, 353-375.

Rayner, N. A., D. E. Parker, E. B. Horton, C. K. Folland, L. V. Alexander, D. P. Rowell, E. C. Kent, and A. Kaplan (2003) Global analyses of sea surface temperature, sea ice, and night marine air temperature since the late nineteenth century, J. Geophys. Res., 108, 4407, https://doi.org/10.1029/2002JD002670.

Schott, F. A., and J. P. McCreary (2001) The monsoon circulation of the Indian Ocean, Prog. Oceanogr., 51, 1–123, doi:10.1016/S0079-6611(01)00083-0.

Schott, F. A., S.-P. Xie, and J. P. McCreary (2009) Indian Ocean circulation and climate variability, Rev. Geophys., 47, RG1002, doi:10.1029/2007RG000245.

Tozuka, T., T. Yokoi, and T. Yamagata (2010) A modeling study of interannual variations of the Seychelles Dome, J. Geophys. Res., 115, C04005, https://doi.org/10.1029/2009JC005547.

Trenberth, K. E. (1984) Signal versus noise in the Southern Oscillation, Mon. Wea. Rev., 112, 326–332, doi:10.1175/1520-0493(1984)112<0326:SVNITS>2.0.CO;2.

Trenary, L., and W. Han (2012) Intraseasonal to interannual variability of South Indian Ocean sea level and thermocline: Remote versus local forcing, J. Phys. Oceanogr., 42, 602–627, https://doi.org/10.1175/JPO-D-11-084.1.

Woodberry, K. E., M. E. Luther, and J. J. O'Brien (1989) The wind-driven seasonal circulation in the southern tropical Indian Ocean, J. Geophys. Res., 94, 17985–18002, https://doi.org/10.1029/JC094Ic12P17985.

Yu, W.D., Xiang, B. Q., Liu, Lin, and Liu, N. (2005) Understanding the origins of interannual thermocline variations in the tropical Indian Ocean, Geophys. Res. Lett., 32 (24), 1-4, doi:10.1029/2005GL024327.

Yu, L., and Weller, R. A. (2007) Objectively analyzed air-sea heat fluxes for the global ice-free oceans (1981-2005), Bulletin of the American Meteorological Society, 88, 527–540. https://doi.org/10.1175/bams-88-4-527.

Zhang, X., and Clarke, A. J. (2015) Observations of Interannual Equatorial Freshwater Jets in the Western Pacific, Journal of Physical Oceanography, 45(11), 2848-2865.

Zhang, X., and Han, W. (2020) Effects of Climate Modes on Interannual Variability of Upwelling in the Tropical Indian Ocean, Journal of Climate, 33(4), 1547-1573, https://journals.ametsoc.org/view/journals/clim/33/4/jcli-d-19-0386.1

Zhuang, W., M. Feng, Y. Du, A. Schiller, and D. Wang (2013) Low-frequency sea level variability in the southern Indian Ocean and its impacts on the oceanic meridional transports, J. Geophys. Res. Oceans, 118, 1302–1315, https://doi.org/10.1002/jgrc.20129.

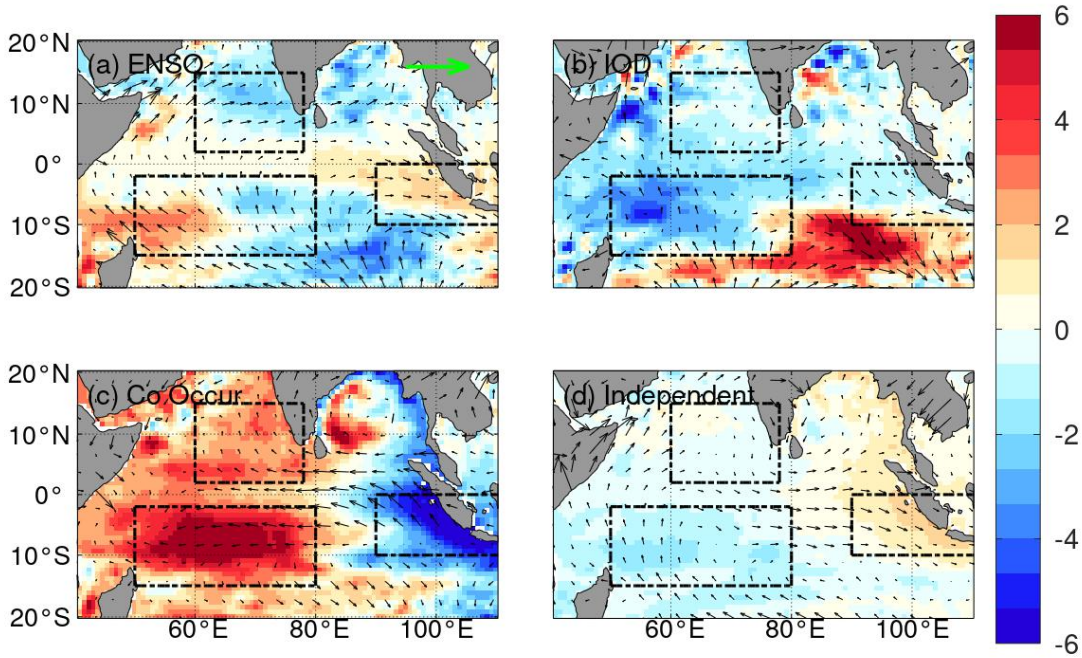

Figure1: The composite of AVISO SSHA (color shading, unit: cm) and wind stress (vectors, unit: N/m^2) for (a) all the pure El Niño years (2002, 2004, 2009), (b) all the pure positive IOD years (2012), and (c) the co-occur years (1994, 1997, 2006, 2015) for the period of 1993 January to 2016 December. (d) is composite of independent years (1993, 1995, 2000, 2001, 2003, 2004, 2005, 2008, 2011, 2012, 2013, 2014, 2016). The composite of SSHA during El Niño years is estimated based on Nov.-Jan. (NDJ) average and the composite of SSHA during IOD years is based on Sept.-Nov. (SON) average.

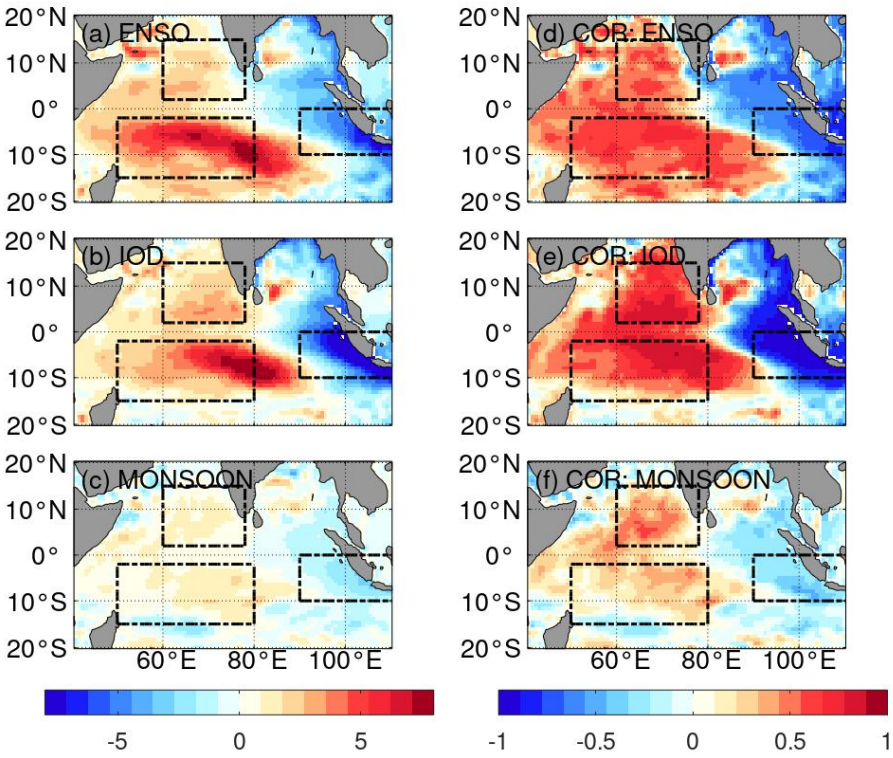

Figure2: Regression of (a) ENSO (b) IOD and (c) Monsoon index (b_1(x,y)×Niño3.4) on SSHA (color shading; unit: cm) for the period of 1993 January to 2016 December. The ENSO index is based on Nov.-Jan. (NDJ) averaged Niño3.4 index, the IOD is based on Sept.-Nov. (SON) averaged DMI index and the Monsoon is based on Jun.-Aug.(JJA) averaged IMRI index. The three box regions are defined in the main text.

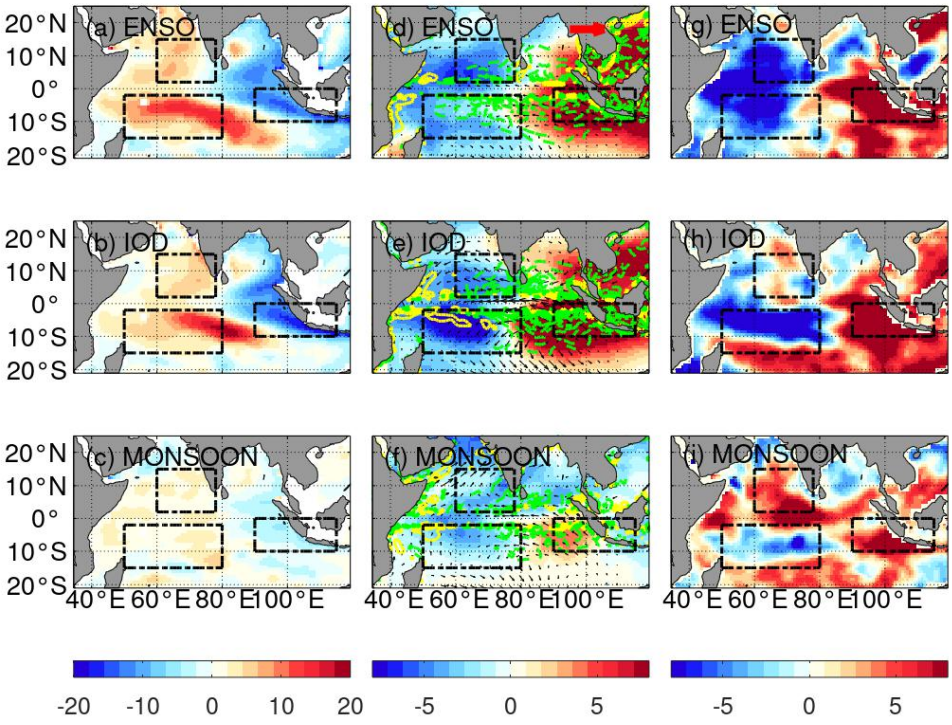

Figure3: Regression of (a) ENSO (b) IOD and (c) Monsoon index (b_1(x,y)×Niño3.4) on D20A (color shading; unit: m), (d)-(f) OLRA (color shading; unit: W/m^2), surface wind (vectors; unit: N/m^2), and Ekman pumping velocity (W_e, line contours), defined as W_e = Curl(/ $_w$f) = (/ x)(^{y}/ $_w$f) − (/ y)(^{x}/ $_w$f). Unit for w_e is 1×10^6 m s^{-1}, and positive (negative) values are in yellow (green), with values of 0.5, 1.5...5.0, (-5.0, -4.5,... -0.5) (g)-(i) surface heat flux (unit: W/m^2) for the period of 1993 January to 2016 December. Net heat flux is a combination of OAFlux and ISCCP, positive means downward. The ENSO index is based on Nov.-Jan. (NDJ) averaged Niño3.4 index, the IOD is based on Sept.-Nov. (SON) averaged DMI index and the Monsoon is based on Jun.-Aug.(JJA) averaged IMRI index. The three box regions are defined in the main text.

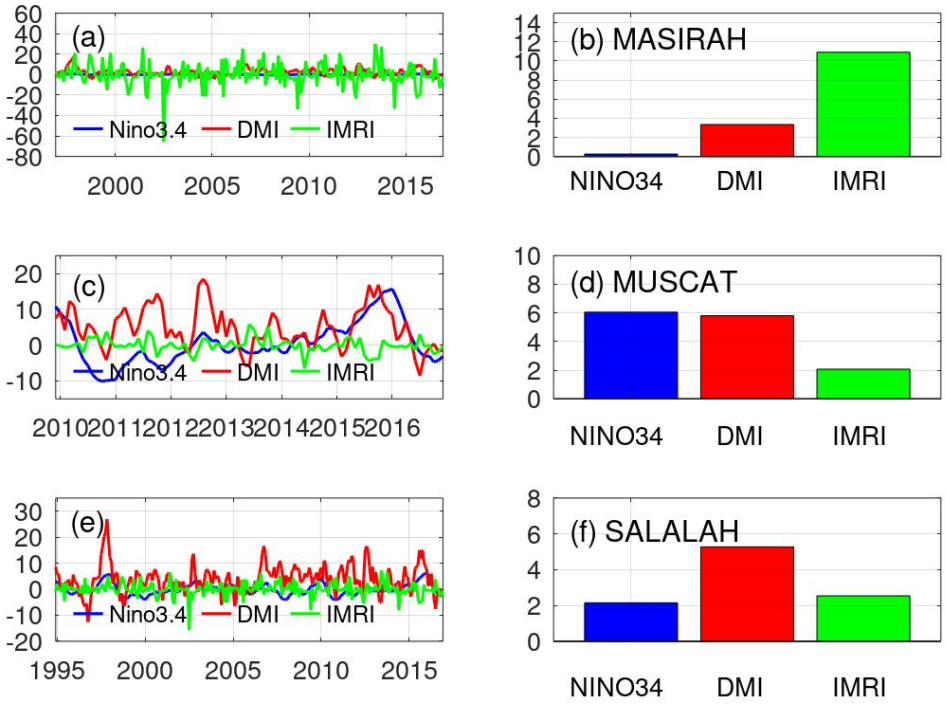

Figure4: ENSO (blue line), IOD (red line) and Monsoon (green line) contribution to insitu sea level at (a) Masirah, (c) Muscat and (e) Salalah for the period of 1993 January to 2016 December. (b), (d), (f) are the standard deviations for each component.